Composites Part B 207 (2021) 108583

Contents lists available at ScienceDirect

Composites Part B

journal homepage: www.elsevier.com/locate/compositesb

Carbon nanotubes and expanded graphite based bulk nanocomposites for de-icing applications

L. Vertuccio [a,*], F. Foglia [a], R. Pantani [a], M.D. Romero-Sánchez [b], B. Calderón [b], L. Guadagno [a,**]

[a] Department of Industrial Engineering, University of Salerno, Via Giovanni Paolo II, Fisciano, (SA), Italy
[b] Applynano Solutions S.L. Parque Científico de Alicante, Naves de apoyo, 3., 03005, Alicante, Spain

ARTICLE INFO

Keywords:
Self-responsive resins
De-icing
Expanded graphite
Electrical conductivity
Joule effect

ABSTRACT

This work deals with the design of bulk nanomaterials able to provide ice protection in different applications ranging from civil to aerospace and automotive engineering. Bulk nanomaterials containing dispersed electrically conductive nanoparticles have been formulated. The heating performed through the Joule effect represents an efficient strategy to rapidly contrast extreme cold and humidity conditions, to reduce environmental pollution and to control rheological properties during the process. The effectiveness of the Joule effect has been evaluated for the same resin, characterized by low values of viscosity, containing incorporated carbon nanotubes and two different grades of expanded graphite. The comparison among the chosen fillers highlights that the nanocomposite containing incorporated the unidimensional filler reaches higher temperatures for lower values of the applied voltage. Graphite nanoplatelets can be advantageously used to reduce the viscosity of the nanomaterials. A higher expansion of the graphite allows for obtaining better performance in the heating efficiency.

1. Introduction

The use of epoxy resin-based composites began in the last century with the first applications in the field of aeronautical, mechanical and naval engineering. Recently, the remarkable properties of these materials, and the decrease of the production cost, are also advantageously exploited in the restoration and structural adaptation of reinforced concrete elements or in masonry. Carbon Fibers Reinforced Polymers (CFRPs) have been employed in civil engineering for the realization of assemblable structures, such as bridges and footbridges, offshore structures, and the construction of experimental buildings. In particular, the applications in the civil sector have mainly consisted on the assembly of pultruded profiles, which use can lead to a reduction of the structural masses up to 70% compared to traditional materials and ensure very short assembly times without requiring excessive use of manpower and/or heavy equipment [1]. It is easy to imagine that these types of materials, due to their considerable lightness, durability, mechanical and anticorrosive performance, will be advantageously used for the construction of light terraces and light roofs also on pre-existing buildings and houses. The use of nanoparticles in the resin enhances the anticorrosive and durability properties [2–4] without affecting the lightness and making the material "smart" [5–8]. Conductive nanoparticles dispersed in the matrix are able to confer it many required properties, such as anti/de-icing, lightning strike resistance and sensor properties [9–15]. Furthermore, this kind of filler, with specific functionalizations, in combination with carbon fibers is able to enhance electrical and thermal properties of electro-activated polymeric shape-memory nanocomposites [16,17]. This paper focuses on the design of structural resins which can be easily activated for the anti/-deicing function. The possibility to integrate this function in epoxy resin makes these systems applicable in civil engineering (bridges, terraces, roofs, etc. exposed to adverse weather conditions). The study performed here is not only limited to the civil engineering sector. In fact, the need for aircraft deicing is a well-known issue. In extreme cold and humidity conditions, it is of crucial importance for the safe take-off of an aircraft to remove and/or preventing a build-up of snow and ice on the wings, tail, etc. The ice on these components may cause changes in their shape, negatively affecting airflow across the surface and hindering the ability to create lift or maintain the aircraft control [18,19]. When ice, snow, or frost are accumulated on an aircraft in the rest condition, usually a

* Corresponding author.
** Corresponding author.
E-mail addresses: lvertuccio@unisa.it (L. Vertuccio), ffoglia@unisa.it (F. Foglia), rpantani@unisa.it (R. Pantani), md.romero@applynano.com (M.D. Romero-Sánchez), blanca.calderon@applynano.com (B. Calderón), lguadagno@unisa.it (L. Guadagno).

https://doi.org/10.1016/j.compositesb.2020.108583
Received 26 September 2020; Received in revised form 25 November 2020; Accepted 15 December 2020
Available online 17 December 2020

deicing fluid, generally a mixture of glycol and water, is heated and sprayed under pressure on the surface of the aircraft components for removing ice and snow before the take-off. After take-off, other approaches may be used to provide de-icing functions. For example, in modern aircraft, mechanical methods are used that allow the breaking of ice on the wing leading edge through the use of an inflatable elastomeric membrane, known as a "Boot," [20] or thermal systems, limited to turbine aircraft, in which the hot air from one of the turbine is diverted to heat the airfoil leading edges [21]. Alternative environmentally-friendly solutions able to save energy can be used to avoid pollution of airport pavements and facilitate and speed up the defrosting operations. Furthermore, these same solutions can be very effective also during service conditions. Recently, efficient strategies based on the Joule effect have been proposed to activate de-icing or anti-icing. Heating flexible films, acting as a heater element, that can be placed as a coating on the surface of the composite, or between layers in the laminate of a Carbon fiber Reinforced Composites (CFRCs) have been proposed by Vertuccio et al. [14]. In the aeronautical sector or other engineering sectors, it has been demonstrated that CNTs can determine criticalities in the obtainment of a suitable homogeneous flexible film/heater. It has been confirmed that, differently from the CNTs, exfoliated/expanded graphites can be easily and advantageously applied. Also, the integration in the composite of a self-regulating heating layer composed of a piezoresistive HDPE/GNP nanocomposite film can provide additional functionalities to the composites, like strain or damage sensing as well as the ability of de-icing without affecting internal structure and performance of the laminate [22]. A mechanically robust superhydrophobic coating for aeronautical composite against ice accretion and ice adhesion has been recently developed [23]. Together with these new strategies, other methods are under investigation. The possibility to use, for the impregnation of the composite, a resin which allows a better transfer of the heat to perform de-icing or prevent it, may be of great benefit to integrate deicing function and also other functional properties [5,14,24–31]. In this paper, the efficiency of the Joule effect in the heating of bulk nanomaterials has been analyzed for three different types of nanocomposites containing incorporated MWCNTs and expanded graphites (EXPG1 and EXPG2). These bulk nanomaterials can be used for the impregnation of GFRPs or CFRPs or in the form of coating. The employed graphites strongly differ among them on the aspect ratio. The performed tests highlight that this last parameter significantly affects the achieved value of temperature for higher values of applied power. The resin containing MWCNTs has proven to be the best performing system both in terms of applied voltages and maximum temperature achieved by the sample. Expanded graphites, instead, can be advantageously applied to maintain low the viscosity of the nanomaterials during the processing stages.

2. Experimental

2.1. Materials and methods

Epoxy resin composites have been obtained using the carbon nanotubes GRAPHISTRENGT C 100 (ARKEMA Colombes, France), the expanded graphite EXPG1 and EXPG2 (Superior Graphite Co. USA). CNTs Graphistrength C 100 and expanded graphite EXPG1 and EXPG2 are available in large quantity from the manufacturer. CNTs are produced through the heterogeneous Catalytic Chemical Vapor Deposition (CCVD) process using a fluidized bed operating in a continuous way. To be independent of the source of Ethylene, CNTs' manufacturing process consists of 2 steps: 1 Ethanol dehydration on alumina catalyst above 350 °C, at atmospheric pressure. This step involves the vaporization of Ethanol, reaction, condensation of water, and Ethylene cooling. 2. Catalytic cracking of Ethylene to CNTs and hydrogen between 600 and 750 °C and atmospheric pressure. The catalyst (Fe_2O_3/Al_2O_3), Ethylene, and partially recycled hydrogen are fed in the lower part of the reactor whereas hydrogen exit at the top and CNT overflow on the side of the disengagement area. After cooling the MWCNT is transported pneumatically on a dense phase (off-gas treatment). On very large facilities off gas (85 vol % H_2) can be valorized as Hydrogen source (as it is or after purification in a PSA plant) or burned in order to produce steam or to heat the MWCNT fluidized bed. Hydrogen availability is an effective path to address global challenges e can be used to minimize global warming by promoting hydrogen-based green economy. Two grades of expanded graphite in the form of powders characterized by high purity have been used as fillers. They are characterized by low moisture content, high consistent carbon content (>99.9%), well-defined particle size distribution, good compressibility and lubricating properties. The filler characteristics are shown in Table 1. The components of epoxy resin are supplied by Gurit (Holding Wattwil, Switzerland). In particular, the precursor is based on the "3,4 Epoxycyclohexylmethyl-3′,4′-epoxycyclohexane carboxylate" (ECC), whereas the hardener agent is based on the "Methyl hexahydrophthalic anhydride" (MHHPA). This system was chosen because, if compared to other traditional systems based on DGEBA/TGMDA precursors and aromatic amines [32,33], is characterized by lower viscosities, short processing times and less drastic "curing temperatures" simultaneously preserving the mechanical performance typical of the traditional systems [34]. The nature of the employed formulation allows saving energy not only during traditional curing cycles but also during unconventional curing processes, such as electrocuring cycles, which may be used to manufacture component or devices with complex geometry [34].

To obtain a uniform dispersion, the fillers have been embedded into the precursor by using an ultra-sonication treatment for 20 min (Hielscher model UP200S-24 kHz high power ultrasonic probe). The required amount of hardener has been added to filler/precursor mixture with a ratio by weight precursor/hardener of 1/1. The obtained mixtures have been mixed by magnetic stirring for 20 min at room temperature and subsequently degassed for 2 h at room temperature. All the mixtures have been cured by a triple curing cycle: 1 h at 80 °C + 20 min at 120 °C + 1 h at 180 °C.

To investigate the heating characteristics of the resin loaded with conductive fillers (CNT expanded graphite), three types of filled samples with a high filler concentration have been obtained. More specifically, a concentration of 3 wt% has been chosen for the carbon nanotube-based system, whereas for both EG1 and EG2 systems the concentration of 7 wt % has been used. The acronyms used here for the three selected systems are EpCNT for the system containing incorporated MWCNTs, and EpEG1, and EpEG2 for the systems containing embedded EG1 and EG2, respectively.

2.2. Experimental set-up and methods

2.2.1. Determination of the sample temperature profiles

The set-up of the experiments carried out to test the heating performance of the formulated nanocomposites is shown in Fig. 1.

Table 1
Characteristics of the fillers.

Characteristics	CNTs	Characteristics	EXPG 1	EXPG 2
Apparent density [Kg/m^3]	50–150	LOI [%]	99.95	99.95
Mean agglomerate size [μm]	200–500	Moisture [%]	<0.1	0.1
Weight loss at 105 °C [%]	<1	Ash [%]	0.05	0.05
C content [wt%]	>90	Scott density [g/ccm]	0.043	0.06
Mean numbers of walls	5–15	Surface area BET [sm/g]	22.0	18.2
Outer mean diameter [nm]	10–15	d10 [μm]	3.3	12.6
Length [μm]	0.1–10	d50 [μm]	9.8	44.4
Aspect ratio [-]	~1000	d90 [μm]	40.2	117

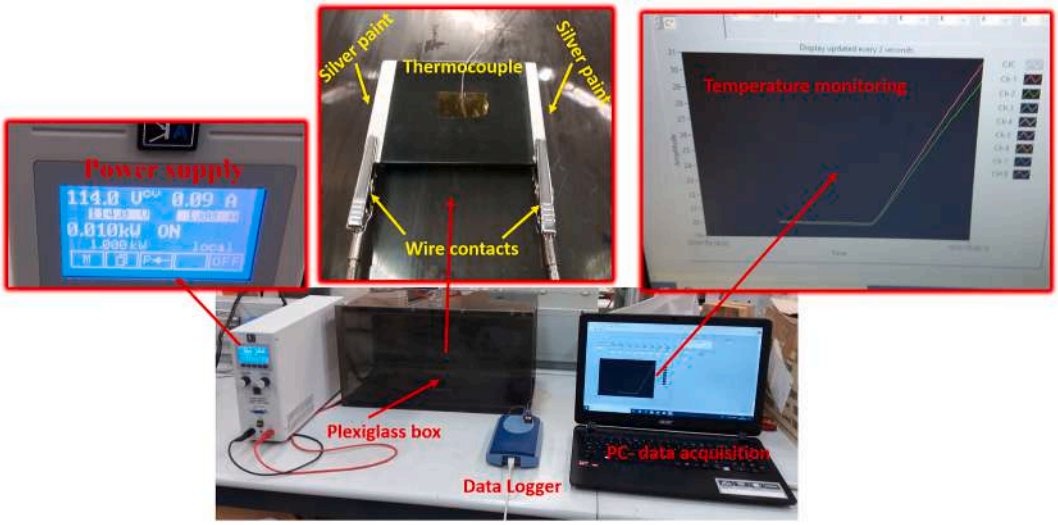

Fig. 1. Experimental setup.

A data acquisition board (Data Logger TC-08 supplied by Pico Technology) was used to acquire the thermocouples measurements. To record the local temperature evolution, a dedicated Labview software was developed. The temperatures were measured using thin wire thermocouples (Type K Omega Engineering Ltd.) with negligible thermal inertia, which were positioned at the center of the sample. The laboratory power supply EA-PSI 8360-10T (Elektro-Automatik, 0–360 V, 0–10 A, 1000W max) was connected to the sample (dimensions 0.35 × 7.5 × 5.0 cm^3) as described in Fig. 1. To reduce possible effects due to surface roughness and to ensure an ohmic contact with the measuring electrodes, the samples were coated by using silver paint (Fig. 1) with a thickness of about 50 μm and characterized by a surface resistivity of 0.001 Ω cm. All measurements were performed in direct current (DC) mode, with a selected constant power. In all the experiments, to reach a steady-state condition, the power was applied for 1200 s. The temperature distribution on the surface of the samples was evaluated by a thermal infrared (IR) Camera (Fluke Ti401 Pro Thermal Imager-WA, USA). The morphology of the expanded graphites was investigated by Transmission Electron Microscopy (TEM) and Field Emission Scanning Electron Microscopy (FESEM). TEM investigation was carried out using a microscope JEOL model JEM-1400 Plus provided with an image acquisition camera model GATAN (ORIUS), and a resolution of 0,38 nm between dots and 0,2 nm between lines. The samples of graphite powders were sonicated before the analysis. FESEM acquisitions were carried out by a FESEM Merlin VP Compact microscope from ZEISS. Suspensions containing the different graphites in a concentration of 0.1 mg/mL in isopropanol were subjected to sonication during 30 min in an ultra-sonication bath. A drop of each suspension was placed on the microscope grip and left to dry before TEM and FESEM analysis. Powder samples were directly located in the FESEM grid without further treatment. DLS analysis of the particle sizes was carried out in a Zetasizer ZSP (Malvern Instrument Ltd., Worcestershire, UK) at 25 °C based on laser Doppler velocimetry and DLS techniques. Previously, the suspension was homogenized using an ultra-sonication probe for a period of 5 min. The refraction index values were set at 1.33 and 2.42 for the dispersant (deionized water) and the material (carbon), respectively. The analysis was carried out by triplicate and the average value and standard deviation were calculated. X-ray photoelectron spectroscopy (XPS, K-ALPHA, Thermo Scientific) was used to analyze the samples surface. All spectra were collected using Al–K_ radiation (1486.6 eV), monochromatized by a twin crystal monochromator, yielding a focused X-ray spot (elliptical in shape with a major axis length of 400 μm) at 3 mA × 12 kV. The alpha hemispherical analyser was operated in the constant energy mode with survey scan pass energies of 200 eV to measure the whole energy band and 50 eV in a narrow scan to selectively measure the particular elements. XPS data were analyzed with Avantage software. A smart background function was used to approximate the experimental backgrounds and surface elemental composition were calculated from background-subtracted peak areas. Charge compensation was achieved with the system flood gun that provides low energy electrons and low energy argon ions from a single source". The samples were mounted on the sample holder and it was analyzed by X-ray Diffraction using a Bruker D8-Advance with mirror Goebel (non-planar samples). The generator of x-ray was a KRISTALLOFLEX K 760-80F (power: 3000W, voltage: 20-60 KV and current: 5–80 mA) with a tube of RX with copper anode. The experimental conditions are: X-ray Tube (40 kV–40 mA); Angular scanning (4–90° 2θ); Step (0.05° 2θ); Preset time (3 s). The electrical conductivity was measured with a two-probe method on specimens with a round shape (2 mm and 50 mm of thickness and diameter, respectively). At least 3 samples were tested for each composition. The electrical contacts were realized on the sample surface with silver paint (RS 196-3600, RS PRO, Corby, UK). The measurements were carried out using an electrometer Keithley 6517A (Keithley Instruments, Cleveland, OH, USA) that acted as power supply and ammeter. The contact resistance has been considered negligible since the measured electrical resistance was in the order of kΩ [35,36]. A rotational rheometer Haake Mars II (Thermo Fisher Scientific Ma,USA), equipped with a parallel plate geometry (25 mm diameter, 1 mm gap), was used to carry out the rheological measurements on the liquid systems. The linear viscoelastic region was determined by strain sweep tests, at the frequency of 1 rad/s. All tests were carried out at 25 °C in oscillatory dynamic mode, in the frequency sweep range from 0.1 to 100 rad/s. FESEM images of nanocomposites loaded with 3% wt/wt of CNTs, 7% wt/wt of expanded graphite EXPG1 and 7% wt/wt of expanded graphite EXPG2 were placed on a carbon tab previously stuck to an aluminum stub (Agar Scientific, Stansted, UK) and were covered with a 250 Å-thick gold film using a sputter coater (Agar mod. 108 A). Nanofilled sample sections were cut from solid samples by a sledge microtome and then the section surfaces were suitably treated, by etching solution, before FESEM investigation. The etching procedure was described in a previous paper [37].

3. Results and discussion

3.1. Characterization of the nanofillers

3.1.1. X-ray photoelectron spectroscopy (XPS)

Surface characterization of CNTs and the expanded graphites has

been carried out by XPS investigation. C1s and O1s scans of the CNTs and graphite samples are shown in Fig. 2. Raw data spectra (red line) are fitted with three components (green, blue and fuchsia peaks) or chemical states.

The elemental composition of CNTs and the graphite samples together with their C/O ratio is shown in Table 2. The samples are characterized by a similar surface composition with different percentages of constituent elements. The expanded graphite EXPG1, compared to the EXPG2 sample, manifests a higher percentage of oxygen, a lower percentage of carbon, and consequently a lower value of the ratio C/O. The percentage of chemical groups on the three samples, determined by XPS, is shown in Table 3. All samples show the presence of a peak at binding energy (BE) of 290.1 (290.6) eV in the spectrum of C1s scan (Fig. 2), which is attributed to a shake-up satellite characteristic of the aromatic carbon, π–π* (HOMO–LUMO) transition. As expected, a higher concentration of C–O bonds is detected for the expanded graphite EXPG1 with respect to the sample EXPG2.

Table 2
Elemental composition of the CNTs and graphites determined by XPS.

Element	MWCNTs	EXPG1	EXPG2
C (%)	98.68	93.81	97.23
O (%)	1.32	6.19	2.77
C/O	74.76	15.16	35.10

Table 3
Percentage of groups of CNTs and graphites determined by XPS.

Bonds	Binding Energy (eV)	MWCNTs	EXPG1	EXPG2
C=C	284.50	87.91	83.03	88.53
C–OH/C-Csp3	285.70	7.78	11.57	7.72
C=O	287.00	2.69	4.35	2.03
Shake up (π–π*)	290.60	1.61	1.04	1.72

3.1.2. *Structural and morphological characterization*

The crystallinity of the samples was analyzed by X-Ray Diffraction (XRD) performed with a Bruker CCD-Apex diffractometer. Fig. 3 shows the XRD profiles of the samples EXPG1 and EXPG2, where the intense 002 reflection, indicating an interlayer distance of 3.39 Å, is observed for both expanded graphites. XRD profiles also show the d-spacings (Å) of 2.12, 2.08, 1.70, 1.23 corresponding to the weaker reflections 100, 101, 004 and 110, respectively. The observed reflections highlight that the crystalline phase of both graphites EXPG1, EXPG2 is hexagonal graphite with ABAB stacking of layers as inferred from a comparison with the theoretical d-spacings calculated and therefore expected for hexagonal graphite [38].

Fig. 3 highlights that no relevant differences are detected in the structure of the crystalline phase of the two graphites. From Scherrer's equation [39], the average in the number of graphene layers has been

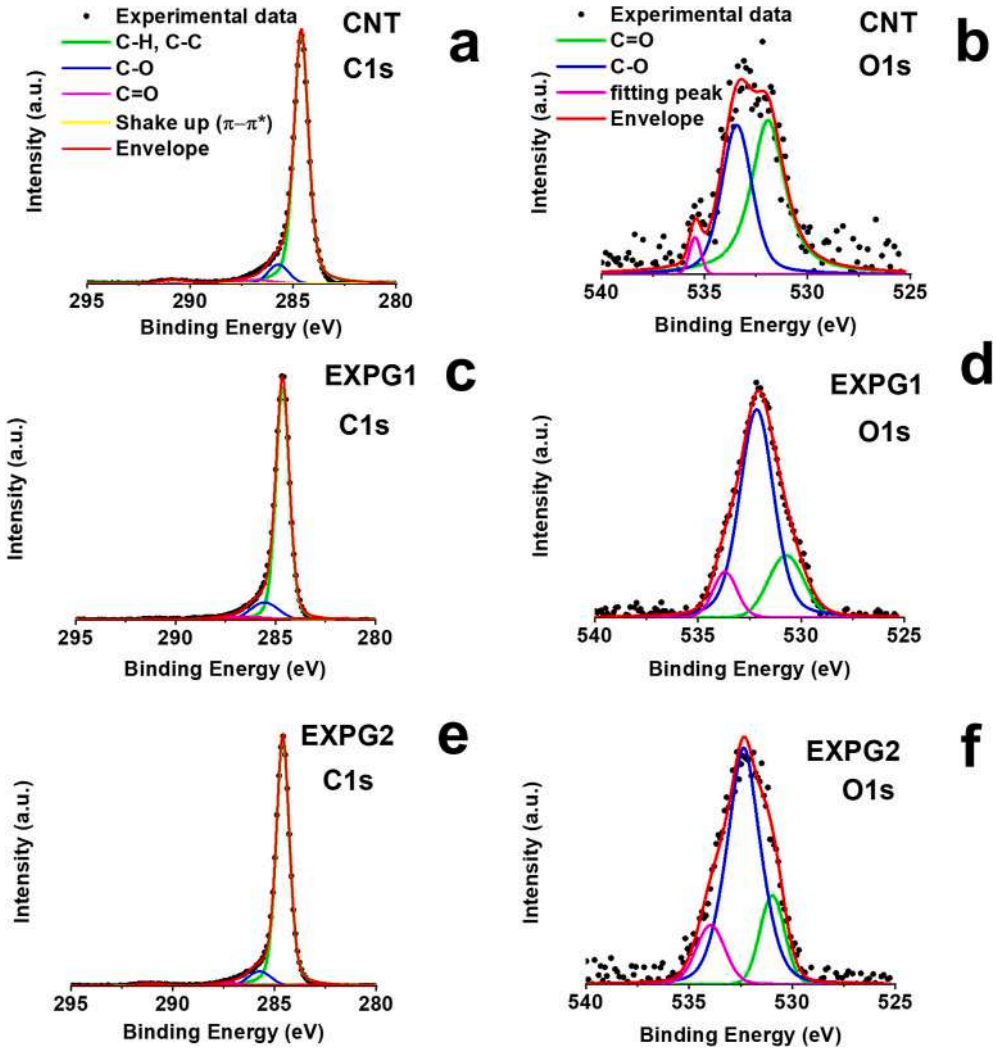

Fig. 2. C1s and O1s scans of the powders of CNTs (a,b); EXPG1 (c,d); EXPG2 (e,f).

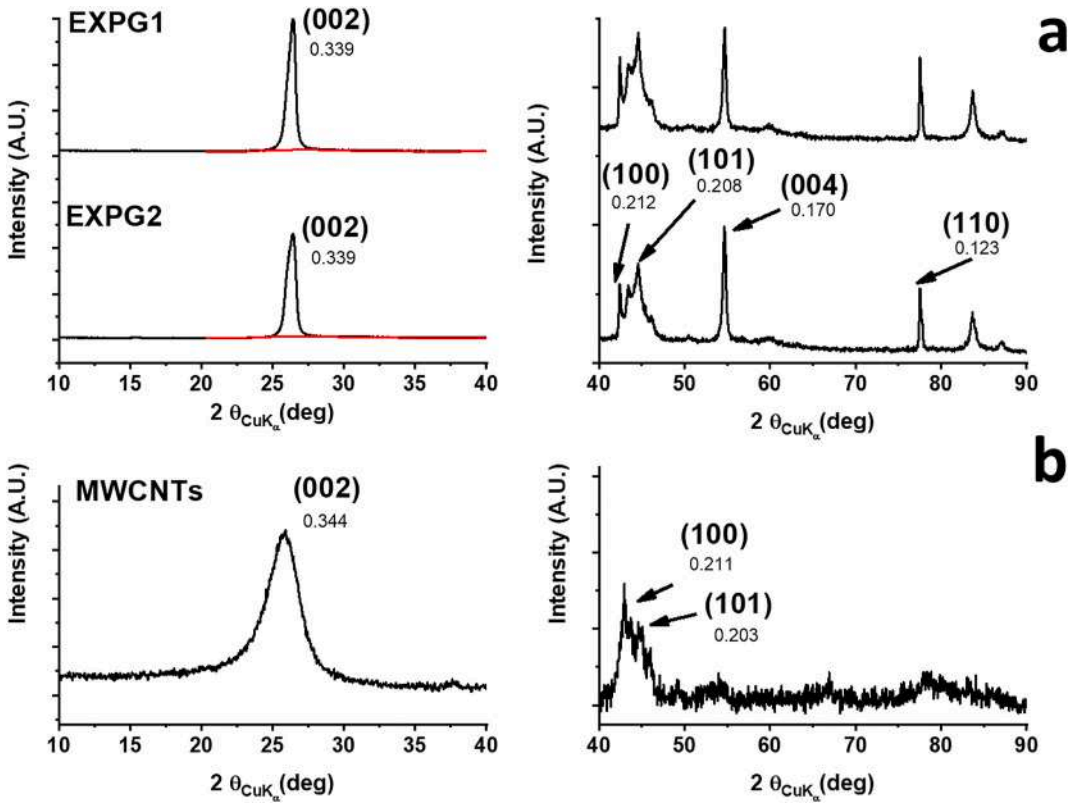

Fig. 3. XRD profiles of:a) EXPG1 and EXPG2 powders; b) MWCNTs.

calculated applying the equation of Ju et al., 2010 [40]:

$$\text{Number of layers} = D_{002}/d_{002} \quad (1)$$

Considering the peak at 26.3 of 2θ (002 reflection), corresponding to the value of 3.39 Å for the d-spacing, an average number of 93 and 76 layers have been obtained for EXPG1 and EXPG2 powder samples, respectively. The two samples are characterized by a high percentage of crystallinity with a very slight decrease for sample EXPG2, for which a crystallinity percentage of 85% has been detected with respect to the very similar value of about 89% detected for sample EXPG1. XRD results have been combined with parameters obtained by morphological investigation to better understand the structural and morphological features of the samples and the differences between the two kinds of expanded graphites. XRD profile of CNTs shows many similarities with the XRD profiles of the expanded graphites for the more intense peaks at 25.9 of 2θ (002 reflection), corresponding to the value of 3.44 Å of the d-spacing, and 42.9 and 44.6 of 2θ (100 and 101 reflections), corresponding to the values of 2.11 Å and 2.03 Å of the d-spacings. The 002 reflection is generated possibly by the reflections from basal hexagonal carbon atomic networks and parallel nanotube stacking layers [41]. The d-spacing value found for this reflection suggests an interlayer spacing of 3.44 Å between individual shells in the multi-wall carbon nanotubes.

3.1.3. FESEM and TEM characterizations

TEM images of the three different fillers are shown in Fig. 4. The values of the geometrical parameters of CNTs here shown (images 4a-b), and other images not reported here, perfectly agree with those displayed in Table 1. TEM images of EXPG1 and EXPG2 graphites (Fig. 4c–d and e-f) highlight that EXPG2 graphite is characterized by larger dimensions of thinner sheets. XRD results previously discussed indicate that the average values of the most likely thickness of the graphite sheets are 31,5 nm and 25,7 nm for EXPG1 and EXPG2, respectively. However, thicker and thinner sheets observed by TEM show a distribution of the thickness, which clearly indicates a higher degree of expansion for sample EXPG2. In particular, also very low values of thickness (around 0.4, 0.9 nm corresponding to 1 or 2 graphene layers) are observed for sample EXPG2, as shown in Fig. 5a. The distribution of the size of EXPG1 and EXPG2 nanoparticles obtained through by Dynamic Light Scattering (DLS) analysis is shown in Fig. 5b.

The fact that EXPG2 powders contain sheets with very few graphene layers is also evidenced by the numerous folded structures present in the powders as shown in the FESEM images (Fig. 6) of expanded graphites EXPG1 (a, b) and EXPG2 (c, d). The lateral dimensions (width and length) of the graphene sheets have been evaluated by FESEM images adopting a statistical value of 50 images. EXPG2 sample frequently shows size values ranging between 29 and 91 μm, whereas in EXPG1 sample the lateral dimension varies between 9 and 31 μm. Size distribution of the nanoparticles detected by Dynamic Light Scattering (DLS) perfectly agrees with the statistical investigation carried out by FESEM investigation.

The combined evaluation of the structural and morphological data allows to deduce the substantial difference between the two different grades of graphite. XRD, TEM, and FESEM data highlight that EXPG2 powder, compared with EXPG1 powder, is characterized by less thick graphite sheets with larger surface areas. The aspect ratio of EXPG2 ranges between 1128 and 3541, whereas that of the EXPG1 sample is between 286 and 984. XPS analysis also evidences that the graphite sheets with higher aspect ratio EXPG2 exhibit lower amount of oxygenated functional groups. The relative content of the edges vs. graphite surface is lower in the graphite EXPG2 with higher aspect ratio. Since the oxygen is mostly attached to the edges, the EXPG2 sample results less functionalized with respect to sample EXPG1.

3.2. Characterization of the nanocomposites

3.2.1. Electrical characterization

The comparison among the Electrical Percolation Threshold (EPT) curves of the epoxy nanocomposites containing dispersed the three

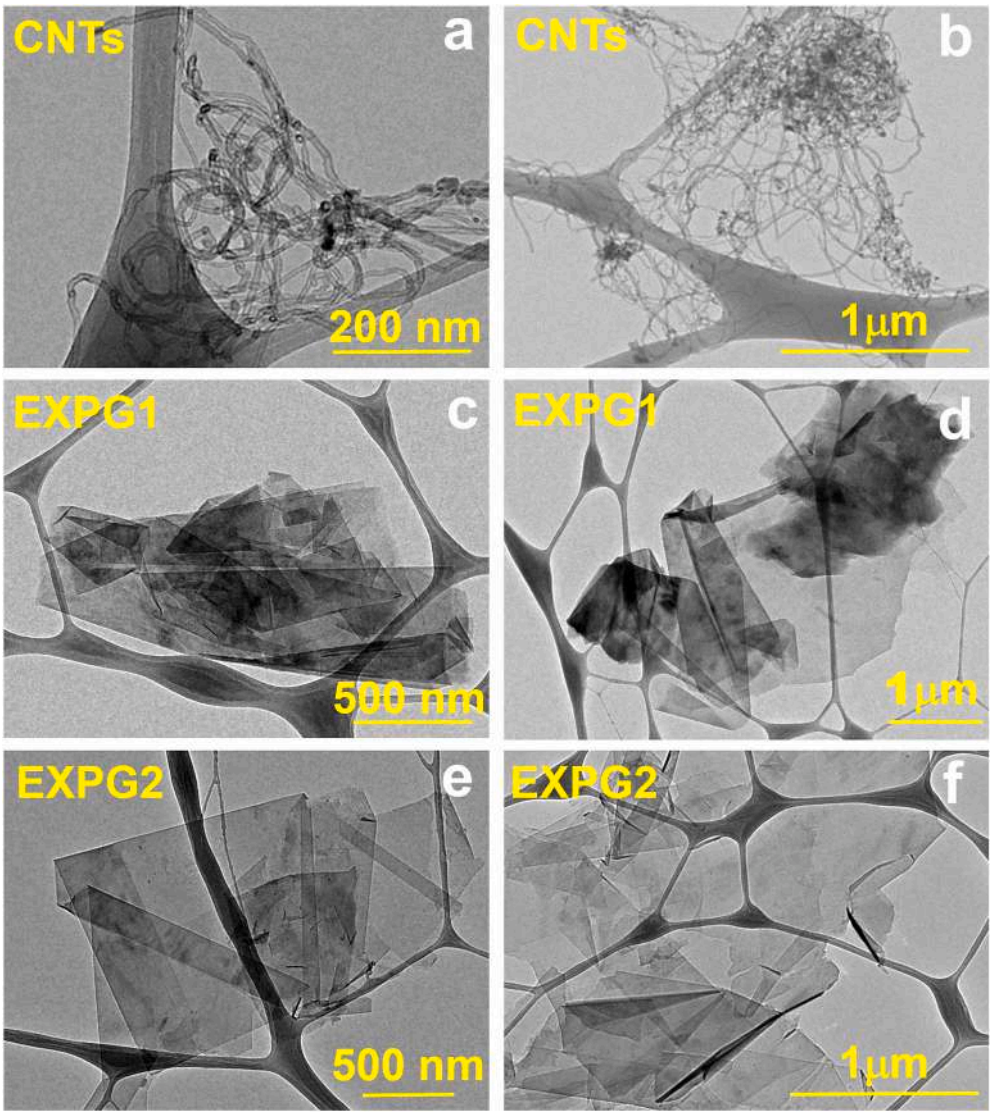

Fig. 4. TEM images of CNTs (a, b) and expanded graphites, EXPG1 (c, d) and EXPG2 (e, f).

different fillers at various concentrations are shown in Fig. 7, together with the optical images of the epoxy nanocomposites loaded with 3% wt/wt of CNTs, 7% wt/wt of EXPG1 and 7% wt/wt of EXPG2, which have been chosen to evaluate the deicing performance. The maximum value considered for the filler concentration has been 7% wt/wt because concentrations higher than 7%, for the sample loaded with EXPG2, are characterized by higher viscosity values and do not guarantee a good filler distribution.

Concerning the EPT range, as expected, the nanocomposite containing CNTs is beyond the EPT also for the low concentration of 0.5% wt/wt, whereas higher concentrations of both expanded graphites are required to achieve the EPT. The system containing embedded the graphite sheets EXPG2 manifests a better electrical performance than the system with EXPG1, both in terms of EPT range and values of electrical conductivity beyond the EPT. It is worth noting that the heating through the joule effect manifests a significant variability in the results depending on the electrical conductivity value of the sample. In fact, the heat generated in the nanofilled resin is due to the flow of electricity through the sample, which implies the loss of part of its energy due to the lattice vibrations (phonons) [42,43]. From Fig. 7, it is possible to observe that for the sample loaded with EXPG1, after the electrical percolation threshold (around 2.0% wt/wt), the electrical conductivity slightly continues to increase up to the concentration of 7.0% wt/wt of nanofiller. Being this concentration that corresponding to the highest electrical conductivity, the concentration of 7% wt/wt of EXPG1 has been chosen for the evaluation of the heating performance. Furthermore, to perform a valid comparison between the two samples loaded with the two kinds of expanded graphite, the same concentration of 7.0% wt/wt of EXPG2 has been considered. Concerning the CNT filler, sample Epoxy-CNT-3% reaches the maximum value of electrical conductivity already at the lower concentration of the nanofiller corresponding to 1.0% wt/wt. The higher concentration of 3.0% wt/wt has been chosen because the thermal conductivity is slightly affected by the nanofiller concentration [44,45]. A higher thermal conductivity allows for a more efficient heat transmission for the same applied voltage. This aspect is particularly relevant for the unidimensional nanofiller, whereas epoxy resins loaded with expanded graphite already manifest higher thermal conductivity with respect to resins loaded with CNTs.

The samples chosen for the electro-heating tests are shown in Fig. 7 (on the right side). These nanocomposites manifest the following values of conductivity: $\sigma = 6.8 \times 10^{-2}$ S/m (Epoxy-CNT-3%); $\sigma = 3.3 \times 10^{-4}$ S/m (Epoxy-EXPG1-7%); $\sigma = 3.2 \times 10^{-2}$ S/m (Epoxy-EXPG2-7%). Usually, the EPT for 1D carbon unfunctionalized nanofiller is lower than covalently functionalized filler [6,32]. Also in this case, where the resin contains embedded 2D fillers, the EPT is slightly lower for the nanocomposites containing a lower amount of oxygenated functional groups

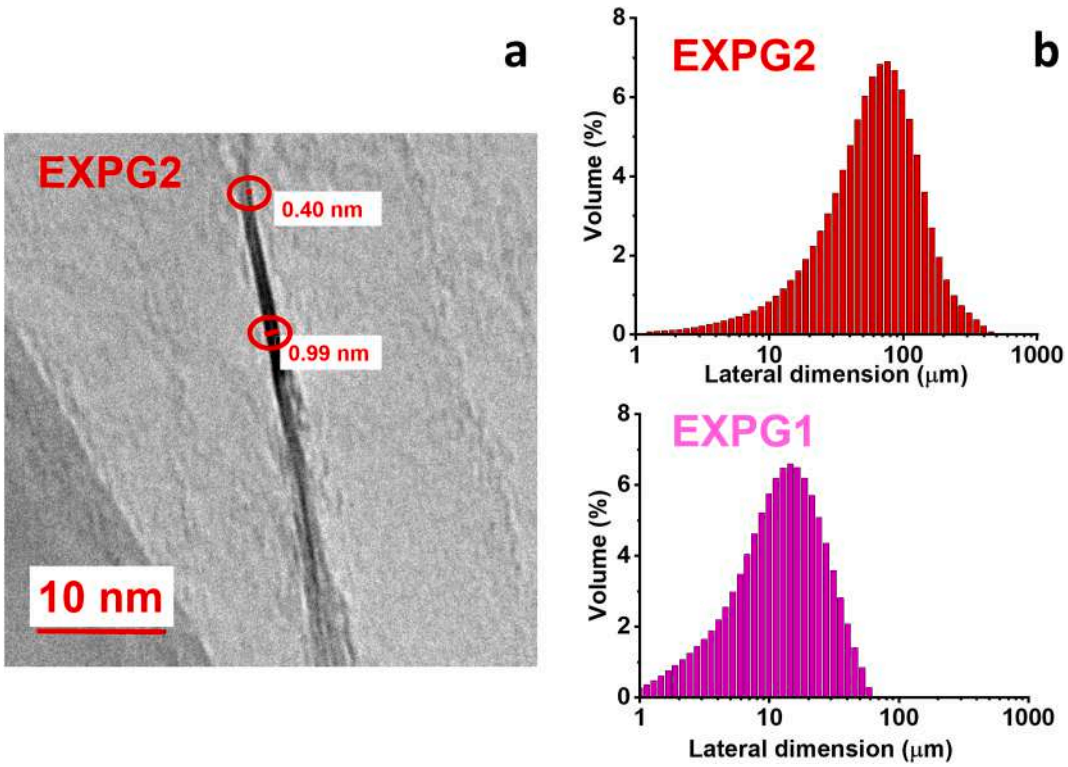

Fig. 5. TEM image of EXPG2 sample, sheet in section (thickness) (a); Average value determined by DLS analysis of lateral dimensions of expanded graphites EXPG1 and EXPG2 (b).

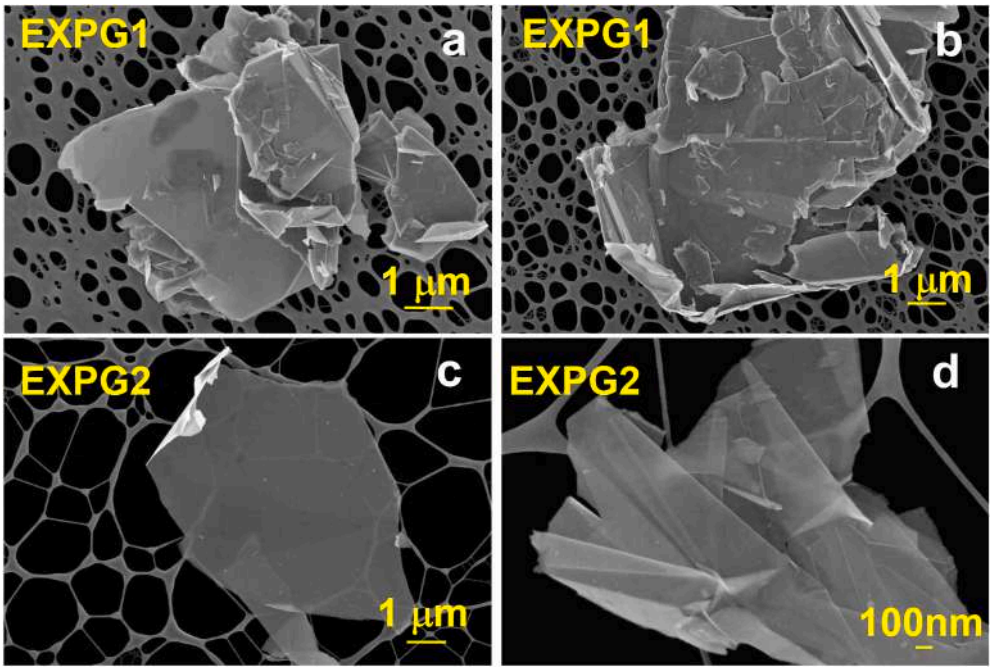

Fig. 6. FESEM images of expanded graphites EXPG1 (a, b) and EXPG2 (c, d).

(EPOXY–EXPG2) as detected by XPS analysis. Furthermore, a lower EPT range for the sample with EXPG2 was expected due to its higher aspect ratio. Similar behavior is also detected for the electrical conductivity. In fact, the value of electrical conductivity, as already found for 1D carbon nanofiller, for the same nanofiller concentration, is higher for the nanocomposite containing the less functionalized filler [6,32,46].

3.2.2. *Morphological characterization of the nanocomposites*

The morphology of the nanocomposites with 7% wt/wt of expanded graphite has been investigated by TEM analysis to understand the influence of the preparation process and the curing cycle on the expansion state of the filler. The images are shown in Fig. 8. The treatments carried out to formulate the nanocomposites do not seem to influence the characteristics already seen for the fillers alone. In fact, from Fig. 8, it is

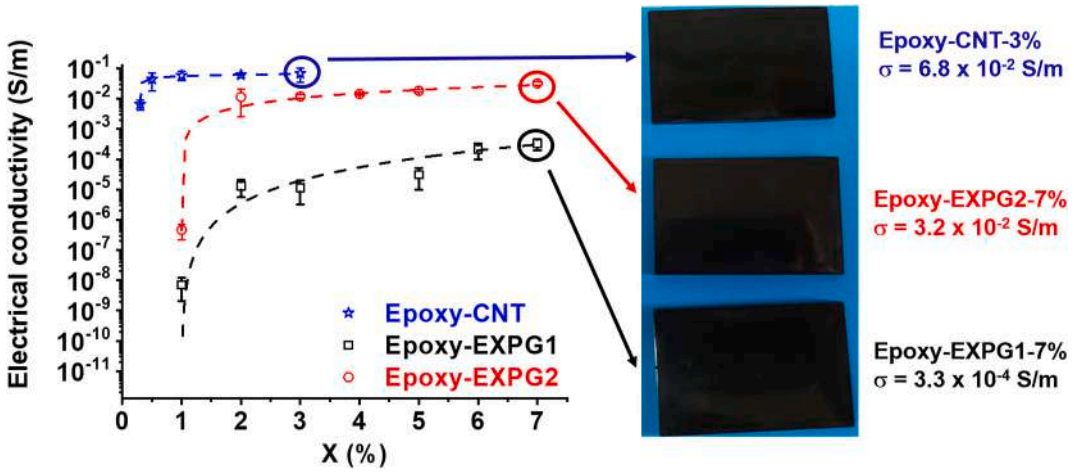

Fig. 7. Electrical conductivity for the Gurit system with CNTs, EXPG1 and EXPG2 (a); optical images of the cured epoxy samples loaded with 3%, 7% and 7% by weight of CNTs, EXPG1 and EXPG2.

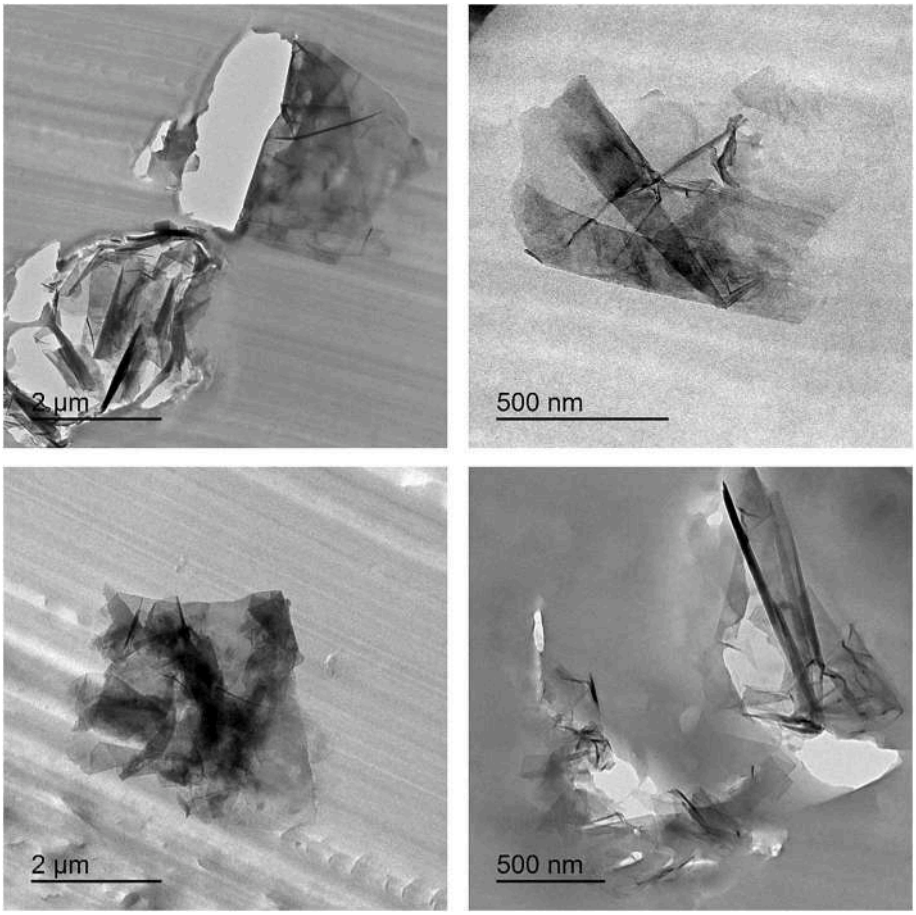

Fig. 8. TEM images of nanocomposites with 7% wt/wt of expanded graphite EXPG1 (on the top) and EXPG2 (on the bottom).

clear that EXPG2 graphite sheets continue to be more expanded and with larger sheet sizes, also when they are embedded in the resin and after the sonication and the curing processes.

The same information can be inferred by the SEM images of Fig. 9, where the surface of the etched samples is shown for each filler. In Fig. 9, it is also possible to analyze the dispersion state of the three fillers. Carbon nanotubes form a dense network homogeneously distributed over the entire surface of the sample. Satisfactory distributions were also observed for the two expanded graphites. The red-contoured ellipses highlight the conductive network determined by the two expanded graphites. It is possible to observe as for the EXPG2 filler, larger sheets are in contact in forming the network with respect to the EXPG1 filler.

3.2.3. Rheological characterization

Viscoelastic properties of unfilled resin and related nanocomposites have been analyzed at 25 °C. The tests have been performed on the fluid complete formulation also including the hardener agent to get as close as possible to real process conditions. To avoid the activation of the

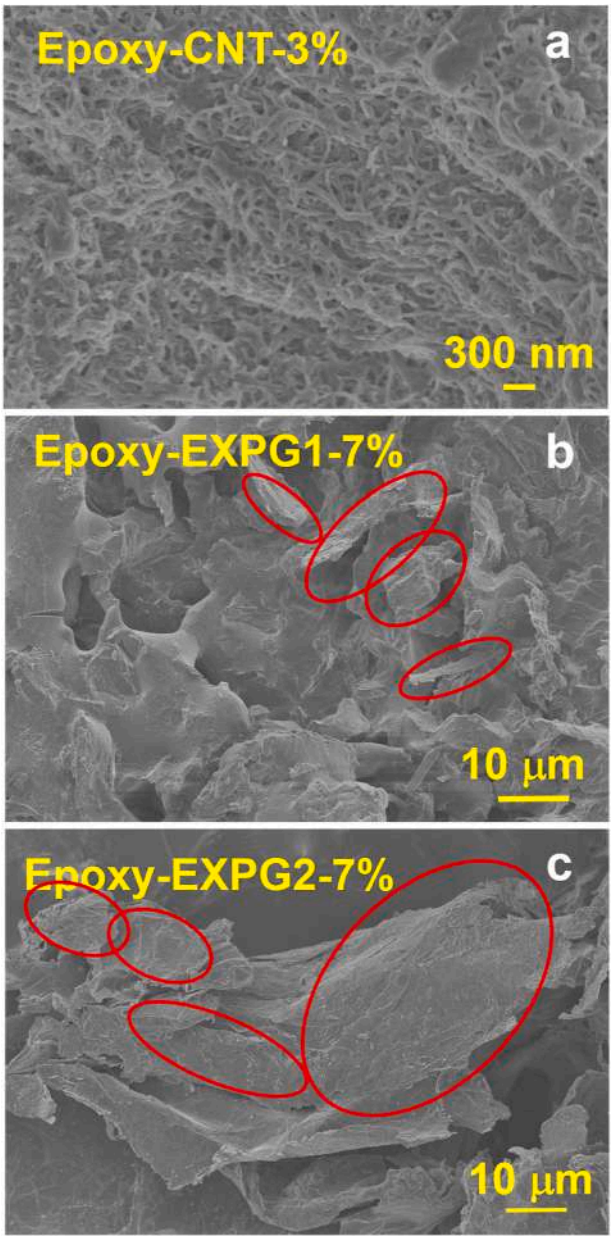

Fig. 9. FESEM images of nanocomposites with 3% wt/wt of CNTs (a), 7% wt/wt of expanded graphite EXPG1 (b) and 7% wt/wt of expanded graphite EXPG2 (c).

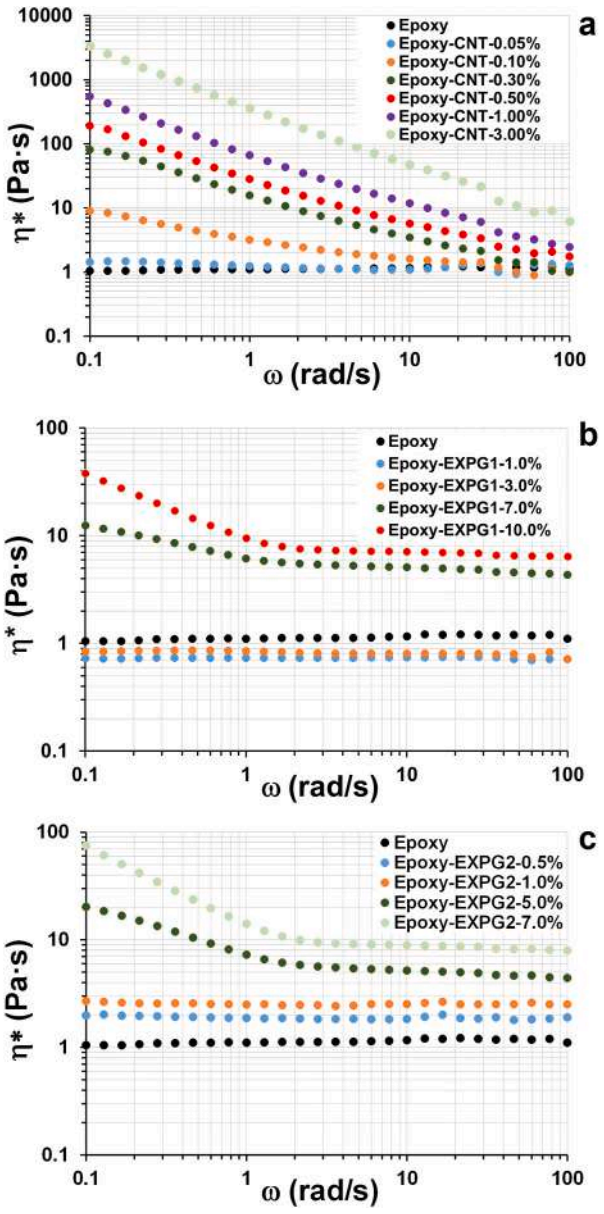

Fig. 10. Complex viscosity vs. frequency of the nanocomposites loaded with different concentrations of CNTs, EXPG1 and EXPG2 nanoparticles.

hardener agent no rheological tests at temperature higher than 25 °C have been performed. The complex viscosity (η*) versus the frequency (ω) of the unfilled epoxy system and the nanocomposites containing the nanofiller dispersed at different concentrations is shown in Fig. 10. Concerning the unfilled epoxy system, the results clearly evidence a Newtonian behavior. The complex viscosity results constant in the whole tested frequency range. The observed trend also highlights that no crosslinking reactions are active or start during the rheological measurements carried out at the chosen temperature. The effect of CNTs on the complex viscosity of the epoxy formulation is shown in Fig. 10a. The dispersion of a small amount of CNTs (0.05% wt/wt) does not seem to modify the behaviour of the nanocomposite with respect to the unfilled resin. Higher amounts of nanotubes, equal to or higher than 0.3% wt/wt, significantly affect the rheological behaviour of the nanocomposite. The complex viscosity clearly manifests a shear thinning behaviour with η* values much higher at the lower frequencies. The behavior of the sample with 0.1% wt/wt of CNTs is intermediate between the sample loaded with 0.05% and 0.3% wt/wt, which corresponds to a well-percolated structure. This trend perfectly agrees with the electrical results (Fig. 7), where it is clearly visible that at the concentration of 0.3% of CNTs, the nanocomposite is located just at the end of the transition insulator-conductor (EPT range). The comparison between electrical and rheological data also highlights that, at room temperature, the rheological percolation threshold falls in the same range as the electric percolation threshold. Much lower viscosity values were obtained for the epoxy system loaded with the two expanded graphites, and between both graphites relevant differences are detected. Fig. 10b evidences that for low EXPG1 amounts (1.0 and 3.0% wt/wt), the graphite sheets act as lubricant additive, even reducing the viscosity with respect to the values of the unfilled resin. This behavior is not manifested by the nanocomposite loaded with the more expanded graphite EXPG2. Furthermore, it is worth noting that the nanocomposite loaded with 1.0 and 3.0% wt/wt of graphite EXPG1 show a Newtonian behavior as the unfilled resin. A concentration of 7% wt/wt corresponds to a percolated structure as also evidenced by the electrical results shown in Fig. 7 for the system loaded with EXPG1. For the system loaded with EXPG2

shown in Fig. 10c, the shear thinning behaviour is already observed for the lower concentration of 5% wt/wt. This is a direct consequence of the different morphological parameters and then of the higher aspect ratio of the EXPG2 filler compared with the EXPG1. Also in this case, the observed behaviour perfectly agrees with the electrical data. In fact, for the system loaded with EXPG2, a lowering in the EPT range is observed respect to that loaded with EXPG1 (Fig. 7) as for the lowering in the rheological percolation threshold. A very relevant aspect of the comparison between rheological and electrical data concerns the correlation between the process difficulties (due to the increase in viscosity determined by the presence of the filler) and the electrical performance required for the nanocomposite. The comparison between data shown here highlights that the nanocomposite can be formulated with CNTs or EXPG2 filler to achieve almost the same electrical conductivity. The systems Epoxy-EXPG2-7% and Epoxy-CNT-3% are characterized by values of electrical conductivity of the same order of magnitude, $\sigma = 3.2 \times 10^{-2}$ S/m and $\sigma = 6.8 \times 10^{-2}$ S/m, respectively. Considering the same requirement for the electrical conductivity, the possibility of working with EXPG2 expanded graphite (even using the filler in larger quantities) allows dealing with mixtures characterized by considerably lower viscosity values.

3.3. Heating performance

Fig. 11 highlights the electrical heating performance of the developed systems. In particular, Fig. 11a shows the temperature profiles of the nanocomposite Epoxy-CNT-3% for applied powers of 3, 5 and 8 W, whereas Fig. 11b and c display the temperature profiles of the nanocomposites Epoxy-EXPG2-7% and Epoxy-EXPG1-7%, respectively for the same values of the applied power. Fig. 11c shows the trend of the curves corresponding to the voltage vs. power. All heating curves have been acquired starting from 25 °C and the measurements were carried out in the air atmosphere. All graphs highlight that the temperature increases rapidly in the first stage with a nearly linear trend to reach a steady-state temperature in which the temperature achieves an equilibrium value.

Table 4 shows the heat flux density, the maximum value of temperature achieved by each sample together with the values of power, applied voltage, and maximum value of temperature (equilibrium value at plateau). The electrical resistance values for the systems loaded with MWCNTs, EXPG1 and EXPG2 are 14.71, 3030.31 and 31.25 Ω m respectively. The three considered systems differ both for the applied voltage values and the temperature achieved for each value of fixed

Table 4
Heat flux density, applied voltage, employed power and maximum value of temperature reached for the 3 systems.

Heat flux density (W/m^2)	Power (W)	Heating rate (°C/s)	Applied Voltage (V)	T_{max} (°C)
		MWCNTs System		
800	3	0.10	67	60
1333	5	0.17	83	75
2133	8	0.24	108	109
		EXPG1 System		
800	3	0.12	190	57
1333	5	0.15	250	70
2133	8	0.25	350	88
		EXPG2 System		
800	3	0.08	160	59
1333	5	0.13	186	70
2133	8	0.21	248	98

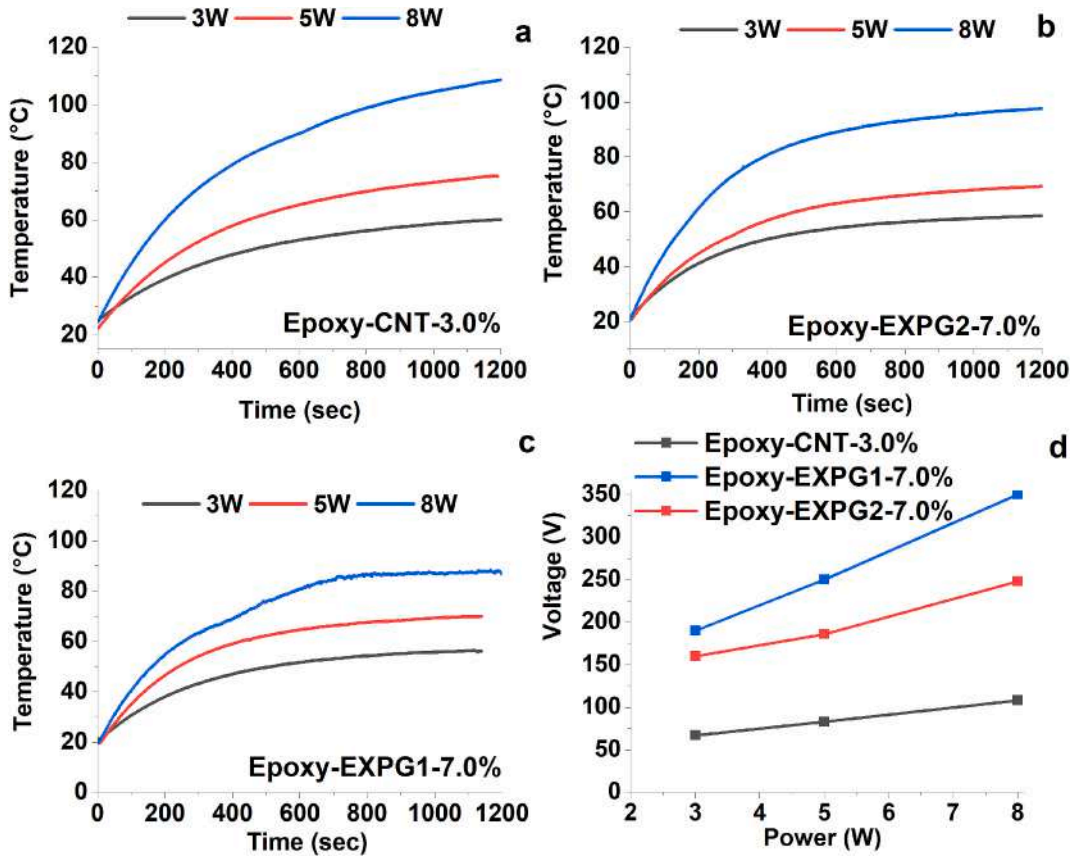

Fig. 11. Temperature-time plots at the applied powers of 3, 5 and 8 W for the systems Epoxy-CNT-3% (a), Epoxy-EXPG2-7% (b) and Epoxy-EXPG1-7% (c); Profile of the voltage curves as a function of the applied power for Epoxy-CNT-3%, Epoxy-EXPG2-7% and Epoxy-EXPG1-7% (d).

power. For each sample, as expected, the heating rate and the temperature achieved in the steady-state increase with increasing the applied voltage and the resulting power.

The systems with carbon nanotubes and expanded graphites, for the same power, reach almost the same values of temperature at the plateau, but voltage values of the CNT based system are lower with respect to those used for systems loaded with expanded graphite. As previously discussed, the system containing CNTs is characterized by a greater electrical conductivity than those corresponding to the systems containing 2D fillers. This allows lower voltage values compared to those used for systems based on expanded graphite for a fixed power rating. The system containing embedded EXPG1, which is characterized by an electrical conductivity value lower of about 2-3 orders of magnitude compared to the other two systems (Fig. 7), reaches, for the same power, lower values in the maximum temperature (with higher applied tensions). The best performance in terms of temperature achieved in the steady-state is manifested by the sample Epoxy-CNT-3%, whereas for the samples containing expanded graphites, the sample loaded with EXPG2 manifests a better behavior in the achieved temperature and the heating rate parameters with respect to the EXPG1 system.

The aspect ratio of the nanofiller does not seem to affect the heating rate of the nanocomposite and the maximum value of temperature achieved in the equilibrium condition, at least for low values of applied power. For the highest value of power instead, the type of nanofiller seems to affect most of all the maximum value of the temperature achieved in the plateau condition. Summarizing, a lower concentration of CNTs (3% wt/wt) determines a nanocomposite able to achieve the temperature of 109 °C for an applied power of 8 W. A higher concentration of expanded graphite EXPG2 (7% wt/wt), characterized by a higher aspect ratio, determines the achievement of a temperature value of 98 °C. For the same nanofiller concentration, a lower aspect ratio of the expanded graphite results in a lower value of the achieved temperature (88 °C). A thermal infrared camera has been used in order to detect the heat transfer process for all considered systems. Fig. 12 shows the temperature mapping of the MWCNTs system during the heating for an applied power 2 W. In particular, the investigation has been performed at different times up to a value of 20 min, for which the steady-state condition is reached (Fig. 12). The temperature values have been obtained as the average temperature detected in the region delimited by the black square line as shown in Fig. 12a. The time sequence of the images denotes a uniform temperature distribution overall sample surface (Fig. 12b).

A similar investigation has been performed for EXPG1 and EXPG2 samples. Fig. 13 shows the images related to the three systems in a steady-state condition, for a power value of 2 W. The EXPG1 system (Fig. 13b) manifests a strong disuniformity in the color tone; the left side of the sample is characterized by a temperature of about 90 °C compared to the center, where a temperature of about 55 °C is detected. On the other hand, the EXPG2 system (Fig. 13c), although presents a small unevenness in the color tones, its temperature is more uniform than the EXPG1 system. Considering that for both samples the power (2 W) and the sample dimensions are the same, the different heating conduction along the surface probably is due to the different size and aspect ratio of the fillers. In fact, if compared with the EXPG1 system, the two systems containing dispersed the fillers characterized by the higher aspect ratio, i.e. carbon-nanotubes and EXGP2, manifest higher electrical conductivity and higher uniform temperature distribution overall sample surface as evident in the three histograms of Fig. 13. In particular, the distribution of the temperature values, detected considering the pixels in the region of the picture, well highlights this behavior. In fact, the surface of the CNT and EXPG2 based systems manifest temperatures between 50 °C and 70 °C, whereas the sample containing EXPG1 shows a strongly decentralized distribution with a long tail that reaches temperature values up to 90 °C.

Also in light of previously characterizations, the best interconnection between the adjacent nanoparticles seems to be strongly affected by the aspect ratio of the filler.

4. Conclusion

In this paper, the development of anti/de-icing bulk systems based on the Joule heating has been described. Three different typologies of carbon nanostructured forms have been employed for the design of the nanocomposites: CNTs and two different grades of expanded graphite. Carbon nanostructured forms, such as CNTs and Graphene-based nanoparticles, embedded inside polymeric materials promise fascinating physics applications, but one of the major obstacles to understand and drive the behavior of the nanofilled polymer towards the desired performance is the absence of a reliable or a single method to produce CNTs or graphene-based nanoparticles such as highly expanded graphite. In literature, graphene and exfoliated/expanded graphite, used to impart functional properties or simply as reinforcement for the polymer, were produced using different procedures and then different structures, functionalizations, and morphological features. For this

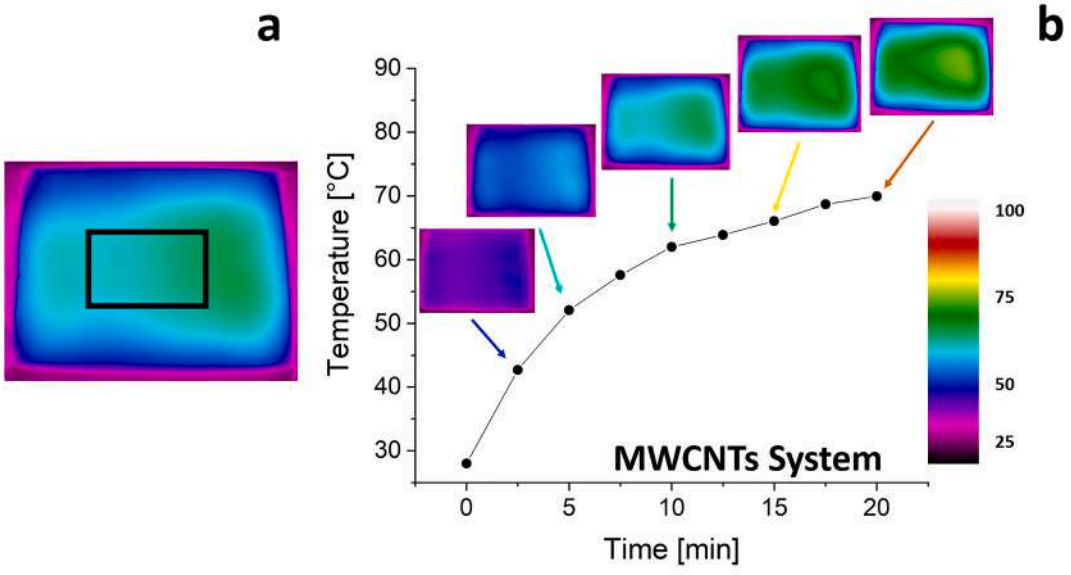

Fig. 12. a) Thermal images of the MWCNTs system; b) time evolution of surface temperature.

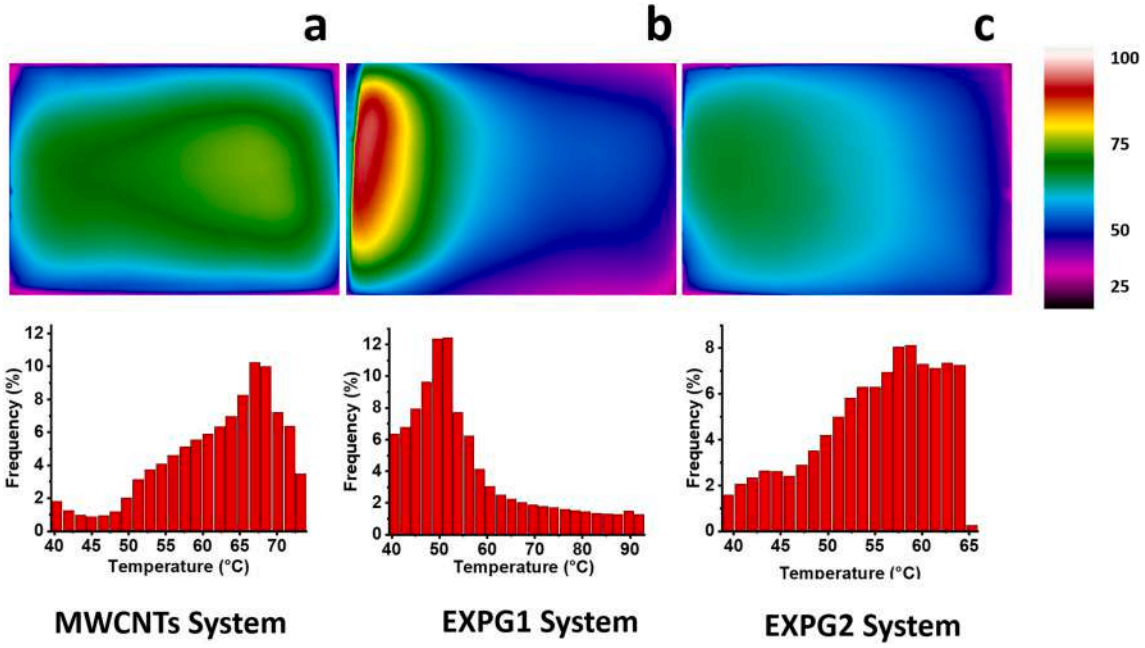

Fig. 13. Thermal images and surface temperature distribution of the samples in steady-state condition: a) MWCNTs system; b) EXPG1 System; c) EXPG2 system.

reason, it is really necessary an accurate characterization of the nanofiller with different techniques to understand the correlations between the structural and morphological organization of nanofiller characteristics and the physical properties resulting for the nanofilled resins. In this paper, an accurate and detailed characterization of the nanofiller was performed before analysing the properties of the nanofilled resins. In particular, an in-depth investigation of the geometric and structural parameters of the nanofillers used in the development of the nanocomposites has been carried out. The morphological and structural investigation highlight that, while no relevant difference are detected in the structure of the crystalline phase of the two graphites, the aspect ratio of the fillers EXPG2 and EXPG1 fall in different ranges, in particular between 1128 and 3541 for EXPG2, and 286–984 for EXPG1. XPS investigation also highlights that the concentration of the oxygenated groups on the nanofiller surfaces is very low for the unidimensional filler (CNTs) and the expanded graphite EXPG2 characterized by higher aspect ratio. This result is compatible with the expected chemical characteristics, the weight of the edges vs. graphite surface is lower in the graphite EXPG2 with a higher aspect ratio. Being most of the oxygen bonded to the edges, the EXP2 sample results less functionalized than the graphite EXPG1. The dimensionality of the filler strongly affects the rheological behavior of the fluid formulations before the curing. The electrical and rheological data highlight a surprisingly strong correlation between the electrical percolation threshold and the rheological one. The nanocomposites containing dispersed CNTs and the more expanded graphite EXPG2 achieve the same electrical conductivity for a different concentration of the filler. Epoxy-EXPG2-7% system and Epoxy-CNT-3% are characterized by similar values of electrical conductivity, $\sigma = 3.2 \times 10^{-2}$ S/m and $\sigma = 6.8 \times 10^{-2}$ S/m. Considering the same requirement for the electrical conductivity, the possibility of working with EXPG2 expanded graphite (even using a higher amount – 7% instead of 3%) allows dealing with mixtures characterized by lower viscosity values. This difference can be very relevant to fix and control process parameters. The best deicing/anti-icing performance is manifested by the resin containing MWCNTs and the more expanded graphite EXPG2. For the highest value of power applied, which determines the achievement of a temperature value ranging between 88 and 109 °C, the nature of the nanofiller affects the value of the temperature achieved at plateau. A lower concentration of CNTs (3% wt/wt) determines a nanocomposite able to achieve the temperature of 109 °C for an applied power of 8 W. A higher concentration of expanded graphite EXPG2 (7% wt/wt), characterized by a higher aspect ratio, determines the achievement of a temperature value of 98 °C. The lowest deicing performance, at the same applied power, is manifested by the nanocomposite with the 2D filler characterized by the lower aspect ratio (88 °C). However, also in this case the temperature of 88 °C guarantees an efficient deicing with the relevant advantage to work with very low values of viscosity during the processing steps.

Credit author statement

L. Vertuccio: Conceptualization, Methodology, Writing - Original Draft, Writing - Review & Editing **F. Foglia:** Investigation, Data Curation, Visualization **R. Pantani:** Review & Editing **M.D. Romero-Sanchez:** Formal analysis, Investigation, Resources **B. Calderón:** Formal analysis, Investigation, Resources **L. Guadagno:** Writing, Review & Editing, Supervision, Project administration, Funding acquisition.

Declaration of competing interest

The authors declare that they have no known competing financial interests or personal relationships that could have appeared to influence the work reported in this paper.

Acknowledgments

This research has been funded with support from the European Union (Horizon 2020 – G.A. EU Project 760940-MASTRO).

References

[1] Abruzzese D, Miccoli L. I nuovi materiali nell'ingegneria civile: i compositi FRP. L'ingegnere edilizia ambiente territorio. 2010. p. 52–4. anno V.
[2] Guadagno L, Naddeo C, Raimondo M, Speranza V, Pantani R, Acquesta A, et al. UV irradiated graphene-based nanocomposites: change in the mechanical properties by local harmoniX atomic force microscopy detection. Materials 2019;12(6):962.
[3] Monetta T, Acquesta A, Carangelo A, Naddeo C, Guadagno L. Enhancement of photooxidative and corrosion resistance of epoxy/graphene water-based coatings on metallic substrate. Prog Org Coating 2019;135:7–18.
[4] Naddeo C, Vertuccio L, Barra G, Guadagno L. Nano-charged polypropylene application: realistic perspectives for enhancing durability. Materials 2017;10(8):943.

[5] Guadagno L, Vertuccio L, Naddeo C, Calabrese E, Barra G, Raimondo M, et al. Self-healing epoxy nanocomposites via reversible hydrogen bonding. Compos B Eng 2019;157:1–13.
[6] Guadagno L, Vertuccio L, Naddeo C, Calabrese E, Barra G, Raimondo M, et al. Reversible self-healing carbon-based nanocomposites for structural applications. Polymers 2019;11(5):903.
[7] Raimondo M, Naddeo C, Vertuccio L, Bonnaud L, Dubois P, Binder WH, et al. Multifunctionality of structural nanohybrids: the crucial role of carbon nanotube covalent and non-covalent functionalization in enabling high thermal, mechanical and self-healing performance. Nanotechnology 2020;31(22):225708.
[8] Shaygan Nia A, Rana S, Döhler D, Jirsa F, Meister A, Guadagno L, et al. Carbon-supported copper nanomaterials: recyclable catalysts for Huisgen [3+ 2] cycloaddition reactions. Chem Eur J 2015;21(30):10763–70.
[9] Raimondo M, Guadagno L, Speranza V, Bonnaud L, Dubois P, Lafdi K. Multifunctional graphene/POSS epoxy resin tailored for aircraft lightning strike protection. Compos B Eng 2018;140:44–56.
[10] Vertuccio L, Guadagno L, Spinelli G, Lamberti P, Tucci V, Russo S. Piezoresistive properties of resin reinforced with carbon nanotubes for health-monitoring of aircraft primary structures. Compos B Eng 2016;107:192–202.
[11] Wang B, Lee B-K, Kwak M-J, Lee D-W. Graphene/polydimethylsiloxane nanocomposite strain sensor. Rev Sci Instrum 2013;84(10):105005.
[12] Wang X, Meng S, Tebyetekerwa M, Li Y, Pionteck J, Sun B, et al. Highly sensitive and stretchable piezoresistive strain sensor based on conductive poly (styrene-butadiene-styrene)/few layer graphene composite fiber. Compos Appl Sci Manuf 2018;105:291–9.
[13] Zha J-W, Zhang B, Li RK, Dang Z-M. High-performance strain sensors based on functionalized graphene nanoplates for damage monitoring. Compos Sci Technol 2016;123:32–8.
[14] Vertuccio L, De Santis F, Pantani R, Lafdi K, Guadagno L. Effective de-icing skin using graphene-based flexible heater. Compos B Eng 2019;162:600–10.
[15] Guadagno L, Foglia F, Pantani R, Romero-Sanchez MD, Calderón B, Vertuccio L. Low-voltage icing protection film for automotive and aeronautical industries. Nanomaterials 2020;10(7):1343.
[16] Lu H, Liang F, Gou J. Nanopaper enabled shape-memory nanocomposite with vertically aligned nickel nanostrand: controlled synthesis and electrical actuation. Soft Matter 2011;7(16):7416–23.
[17] Lu H, Min Huang W. Synergistic effect of self-assembled carboxylic acid-functionalized carbon nanotubes and carbon fiber for improved electro-activated polymeric shape-memory nanocomposite. Appl Phys Lett 2013;102(23):231910.
[18] Goraj Z. An overview of the deicing and anti-icing technologies with prospects for the future. 24th international congress of the aeronautical sciences2004.
[19] Park MS. Aircraft de-icing system using thermal conductive fibers. 2015.
[20] Heinrich A, Ross R, Zumwalt G, Provorse J, Padmanabhan V. Aircraft icing handbook, ume 2. Gates Learjet Corp Wichita KS; 1991.
[21] Parent O, Ilinca A. Anti-icing and de-icing techniques for wind turbines: critical review. Cold Reg Sci Technol 2011;65(1):88–96.
[22] Liu Y, van Vliet T, Tao Y, Busfield JJ, Peijs T, Bilotti E, et al. Sustainable and self-regulating out-of-oven manufacturing of FRPs with integrated multifunctional capabilities. Compos Sci Technol 2020;190:108032.
[23] Tong W, Xiong D, Wang N, Wu Z, Zhou H. Mechanically robust superhydrophobic coating for aeronautical composite against ice accretion and ice adhesion. Compos B Eng 2019;176:107267.
[24] Chu H, Zhang Z, Liu Y, Leng J. Self-heating fiber reinforced polymer composite using meso/macropore carbon nanotube paper and its application in deicing. Carbon 2014;66:154–63.
[25] Debelak B, Lafdi K. Use of exfoliated graphite filler to enhance polymer physical properties. Carbon 2007;45(9):1727–34.
[26] Kausar A, Rafique I, Muhammad B. Review of applications of polymer/carbon nanotubes and epoxy/CNT composites. Polym Plast Technol Eng 2016;55(11):1167–91.
[27] Ma P-C, Siddiqui NA, Marom G, Kim J-K. Dispersion and functionalization of carbon nanotubes for polymer-based nanocomposites: a review. Compos Appl Sci Manuf 2010;41(10):1345–67.
[28] Spinelli G, Lamberti P, Tucci V, Guadagno L, Vertuccio L. Damage monitoring of structural resins loaded with carbon fillers: experimental and theoretical study. Nanomaterials 2020;10(3):434.
[29] Spinelli G, Lamberti P, Tucci V, Vertuccio L, Guadagno L. Experimental and theoretical study on piezoresistive properties of a structural resin reinforced with carbon nanotubes for strain sensing and damage monitoring. Compos B Eng 2018;145:90–9.
[30] Vertuccio L, Guadagno L, Spinelli G, Lamberti P, Zarrelli M, Russo S, et al. Smart coatings of epoxy based CNTs designed to meet practical expectations in aeronautics. Compos B Eng 2018;147:42–6.
[31] Vertuccio L, Vittoria V, Guadagno L, De Santis F. Strain and damage monitoring in carbon-nanotube-based composite under cyclic strain. Compos Appl Sci Manuf 2015;71:9–16.
[32] Guadagno L, De Vivo B, Di Bartolomeo A, Lamberti P, Sorrentino A, Tucci V, et al. Effect of functionalization on the thermo-mechanical and electrical behavior of multi-wall carbon nanotube/epoxy composites. Carbon 2011;49(6):1919–30.
[33] Guadagno L, Vertuccio L, Sorrentino A, Raimondo M, Naddeo C, Vittoria V, et al. Mechanical and barrier properties of epoxy resin filled with multi-walled carbon nanotubes. Carbon 2009;47(10):2419–30.
[34] Guadagno L, Sorrentino A, Delprat P, Vertuccio L. Design of multifunctional composites: new strategy to save energy and improve mechanical performance. Nanomaterials 2020;10(11):2285.
[35] Ku-Herrera J, Aviles F. Cyclic tension and compression piezoresistivity of carbon nanotube/vinyl ester composites in the elastic and plastic regimes. Carbon 2012;50(7):2592–8.
[36] Oliva-Avilés A, Avilés F, Sosa V. Electrical and piezoresistive properties of multi-walled carbon nanotube/polymer composite films aligned by an electric field. Carbon 2011;49(9):2989–97.
[37] Vertuccio L, Russo S, Raimondo M, Lafdi K, Guadagno L. Influence of carbon nanofillers on the curing kinetics of epoxy-amine resin. RSC Adv 2015;5(110):90437–50.
[38] Ganguli S, Roy AK, Anderson DP. Improved thermal conductivity for chemically functionalized exfoliated graphite/epoxy composites. Carbon 2008;46(5):806–17.
[39] Tadokoro H. Structure of crystalline polymers. Krieger Pub Co; 1979.
[40] Ju H-M, Huh SH, Choi S-H, Lee H-L. Structures of thermally and chemically reduced graphene. Mater Lett 2010;64(3):357–60.
[41] Wang Z, Hui C. Electron microscopy of nanotubes. 清华大学出版社有限公司; 2004.
[42] Donati G, De Nicola A, Munao G, Byshkin M, Vertuccio L, Guadagno L, et al. Simulation of self-heating process on the nanoscale: a multiscale Approach for molecular models of nanocomposite materials. Nanoscale Adv 2020;2:3164–80.
[43] Ragab T, Basaran C. Joule heating in single-walled carbon nanotubes. J Appl Phys 2009;106(6):063705.
[44] Romano V, Naddeo C, Guadagno L, Vertuccio L. Thermal conductivity of epoxy resins filled with MWCNT and hydrotalcite clay: experimental data and theoretical predictive modeling. Polym Compos 2015;36(6):1118–23.
[45] Romano V, Naddeo C, Vertuccio L, Lafdi K, Guadagno L. Experimental evaluation and modeling of thermal conductivity of tetrafunctional epoxy resin containing different carbon nanostructures. Polym Eng Sci 2017;57(7):779–86.
[46] Guadagno L, Vertuccio L, Naddeo C, Barra G, Raimondo M, Sorrentino A, et al. Functional structural nanocomposites with integrated self-healing ability. Mater Today: Proceedings 2020. https://doi.org/10.1016/j.matpr.2020.03.051. In press.